Solar Phys (2010) 262: 461–480
DOI 10.1007/s11207-009-9444-4

Automatic Detection and Extraction of Coronal Dimmings from SDO/AIA Data

G.D.R. Attrill · M.J. Wills-Davey

Received: 15 May 2009 / Accepted: 21 August 2009 / Published online: 6 October 2009

Abstract The volume of data anticipated from the *Solar Dynamics Observatory/Atmospheric Imaging Assembly* (SDO/AIA) highlights the necessity for the development of automatic-detection methods for various types of solar activity. Initially recognized in the 1970s, it is now well established that coronal dimmings are closely associated with coronal mass ejections (CMEs), and they are particularly noted as a reliable indicator of front-side (halo) CMEs, which can be difficult to detect in white-light coronagraph data.

Existing work clearly demonstrates that several properties derived from the analysis of coronal dimmings can give useful information about the associated CME. The development and implementation of an automated coronal-dimming region detection and extraction algorithm removes visual observer bias, however unintentional, from the determination of physical quantities such as spatial location, area, and volume. This allows for reproducible, quantifiable results to be mined from very large data sets. The information derived may facilitate more reliable early space-weather detection, as well as offering the potential for conducting large-sample studies focused on determining the geo-effectiveness of CMEs, coupled with analysis of their associated coronal dimming signatures.

In this paper we present examples of both simple and complex dimming events extracted using our algorithm, which will be run as a module for the SDO/*Computer Vision Centre*. Contrasting and well-studied events at both the minimum and maximum of solar cycle 23 are identified in *Solar and Heliospheric Observatory/Extreme ultra-violet Imaging Telescope* (SOHO/EIT) data. A more recent example extracted from *Solar and Terrestrial Relations Observatory/Extreme Ultra-Violet Imager* (STEREO/EUVI) data is also presented, demonstrating the potential for the anticipated application to SDO/AIA data. The detection part of our algorithm is based largely on the principle of operation of the NEMO software, namely the detection of significant variation in the statistics of the EUV image pixels (Podladchikova and Berghmans in *Solar Phys*. **228**, 265 – 284, 2005). As well as running on historic data

Solar Image Processing and Analysis
Guest Editors: J. Ireland and C.A. Young.

G.D.R. Attrill (✉) · M.J. Wills-Davey
Harvard-Smithsonian Center for Astrophysics, 60 Garden Street, Cambridge, MA 02138, USA
e-mail: gattrill@cfa.harvard.edu

sets, the presented algorithm is capable of detecting and extracting coronal dimmings in near real-time.

Keywords Corona, quiet · Coronal mass ejections, low coronal signatures · Instrumentation and data management

1. Introduction

The *Atmospheric Imaging Assembly* (AIA), onboard NASA's *Solar Dynamics Observatory* (SDO), is anticipated to be launched early in 2010. Producing Level 0 data at a rate of 1.1 Tb day^{-1}, the raw data volume from AIA will be made up of eight (one UV and seven EUV) 4096×4096 images every ten seconds. To tackle the volume of data expected from AIA, an international consortium has been selected by NASA to address the requirement for automated feature recognition in SDO images. The companion paper by Martens *et al.* (2009) describes this *Computer Vision Center* (CVC) for SDO. As specified in Martens *et al.* (2009), the output from the CVC will be entered into the Helio Events Knowledgebase. The Virtual Solar Observatory will provide the interface with which the solar community can access the metadata returned by the various modules.

This paper focuses on the description of one component module of the CVC, designed to automatically detect and extract coronal dimmings and associated metadata from AIA images. Coronal dimming is expected to be observed in the seven EUV AIA bandpasses (94, 131, 171, 193, 211, 304, and 335 Å). Our automated coronal-dimming region detection and extraction algorithm performs several useful functions: In addition to processing the considerable volume of data, the automated technique is desirable as it removes visual observer bias from both the identification of coronal dimmings and ultimately the determination of related physical quantities (see, *e.g.,* Wills-Davey, 2006). The metadata returned by our algorithm includes location coordinates, area, volume, mass, and information on the dynamics of coronal dimmings, and will allow solar scientists to effectively use the data returned by SDO. Coronal dimmings are of particular interest to the scientific space-weather community, as they are closely associated with coronal mass ejections (CMEs).

Automated methods return reproducible, quantifiable results which can be mined from very large data sets. As well as running on historic data sets, the algorithm described in this paper is capable of detecting and extracting coronal dimmings in near real-time.

1.1. Observations of Coronal Dimmings

Coronal dimmings are usually observed as decreases in intensity in soft X-rays (Hudson, Acton, and Freeland, 1996; Sterling and Hudson, 1997) and extreme ultra-violet (EUV) data (Thompson *et al.*, 1998). They appear relatively suddenly, on timescales of minutes. The cause of coronal dimmings has been much debated in the literature, and there are two generally accepted possibilities:

i) The dimming may be due to a density depletion caused by an evacuation of plasma (Hudson, Acton, and Freeland, 1996). Such an effect may be caused by the eruption of the local magnetic field, leading to considerable expansion of magnetic loops into interplanetary space. The expansion creates a larger volume, leading to a region of decreased plasma density as a result.

ii) Although plasma evacuation is a widely accepted interpretation of the dimming signature, it should be noted that a decrease in intensity in coronal plasma may be caused by

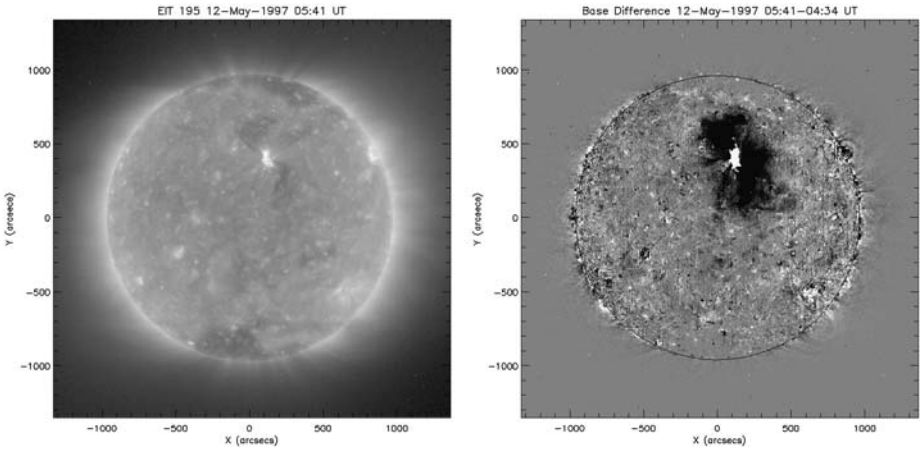

Figure 1 Left panel: An example of an original EIT intensity image showing two dimming regions near the post-eruptive arcade. Right panel: The corresponding base – difference image. The dimming regions are the black areas. Regions that do not show any significant change in intensity with respect to the pre-event (base) image appear gray.

a change in temperature as well as by density depletion (*e.g.,* Thompson *et al.*, 1998; Chertok and Grechnev, 2003). Differences observed between images in different emission lines suggest that some secondary temperature variations may also be responsible for the appearance of dimmings. However, Hudson, Acton, and Freeland (1996) showed that the timescale of the dimming formation observed in *Yohkoh*/SXT data is much faster than corresponding conductive and radiative cooling times, which suggests that the dimmings are primarily a result of density depletion rather than a temperature effect.

1.2. Studying Coronal Dimmings

Although coronal dimmings can be detected in calibrated intensity images of the corona, they are preferentially studied using "base – difference" images. These images have a pre-event image subtracted from all subsequent frames. Thus increases in intensity (with respect to the pre-event image, see also Chertok and Grechnev, 2005), appear white and relative decreases in intensity appear dark (black). Figure 1 shows an example of an original EIT intensity image and its corresponding base – difference image. Regions that do not show any significant change in intensity with respect to the pre-event (base) image appear gray. In this example, it is possible to identify the dimming regions in the original intensity image, although this is not always the case.

It should be emphasized that base-difference images show real intensity changes with respect to the pre-event image. Thus the appearance of dimmings can be created by displacement (not necessarily removal) of a bright coronal structure, revealing the quiet-Sun emission underneath (Rust and Hildner, 1976). In such a case, plasma evacuation would not be a correct interpretation of the dimming signature. On the other hand, a large-scale loop may well erupt and become a constituent of a CME. In this case the dimming signature would be the same as for the displaced loop, although a deeper dimming at the footpoints of the erupted loop may be expected as the loop is expanded and plasma evacuated from the region. The point is that the only way to ascertain whether or not the bright structure has erupted or simply moved, is to study the original intensity data that corresponds to the dimmed environment identified in the base – differenced data.

1.3. How Are Coronal Dimmings Related to CMEs?

Although coronal dimming has long been closely associated with CMEs (*e.g.,* Rust and Hildner, 1976) and dimmings are now widely acknowledged as a reliable indicator of front-side CMEs (Thompson *et al.*, 2000; Hudson and Cliver, 2001), the CME – dimming association was only confirmed recently using a statistical analysis (Bewsher, Harrison, and Brown, 2008). In "double dimming" events (*e.g.,* 7 April 1997, 12 May 1997), it was suggested that the dimmings mark the position of the footpoints of an erupted flux rope that makes up the core magnetic field of the associated CME (Hudson and Webb, 1997; Sterling and Hudson, 1997; Webb *et al.*, 2000).

Assuming that the CME is mostly rooted in the dimmings, several properties derived from the study of dimmings can be used to obtain information about the associated CME:

i) estimates of the volume of dimmings and calculations of the emission measure can give a proxy for the amount of plasma making up the CME mass (Sterling and Hudson, 1997; Wang *et al.*, 2002; Zhukov and Auchère, 2004), since the optically-thin EUV emission is proportional to the density squared. Although large uncertainties are associated with estimates of coronal mass loss (due to the dependence of calculations on the emission measure distribution, which is not well known, and uncertainties in estimating the volume of the dimming regions, due in part to the obscuring effect of the bright post-eruptive arcade on nearby dimmings; Hudson and Webb, 1997; Attrill *et al.*, 2006; Aschwanden *et al.*, 2009), the results do suggest that at least part of the CME mass comes from coronal dimming regions. Harrison and Lyons (2000) conclude that the mass evacuated from the dimming regions may account for much of the mass of the outer shell of the CME;

ii) the spatial extent of coronal dimmings can give information regarding the angular extent of the associated CME (Thompson *et al.*, 2000; Attrill *et al.*, 2007);

iii) quantitative measurement of the magnetic flux through dimmings can be compared to the magnetic flux of modeled magnetic clouds (MC) at 1 AU (Webb *et al.*, 2000; Mandrini *et al.*, 2005; Attrill *et al.*, 2006; Qiu *et al.*, 2007; Démoulin, 2008);

iv) studying the evolution of the dimmings, particularly during their recovery phase, can give information about the evolution of the CME post-eruption (Attrill *et al.*, 2006);

v) the distribution of the dimmings, their order of formation and measurement of their magnetic-flux contribution to the associated CME enabled Mandrini *et al.* (2007) to derive an understanding of the CME interaction with its surroundings in the low corona during its formation phase, for the case of the complex 28 October 2003 event.

1.4. Types of Dimming and Focus of Our Algorithm

There are a wide variety of observed dimming signatures: For example, Hudson and Webb (1997) categorized four different types of dimmings observed in soft X-ray data. Despite the oft-assumed interpretation that coronal dimmings mark the footpoints of an erupted flux rope, Mandrini *et al.* (2007) showed that coronal dimmings are not always a simple signature of ICME footpoints. This variety presents a challenge to developing robust, automatic detection and extraction methods.

In EUV data, there is almost always some kind of coronal dimming present on the solar disk at any given time (D. Bewsher, private communication, 2009). However, the type of dimming associated with a CME may be specifically distinguished as "eruptive dimmings". It is this class of dimming that our algorithm is designed to detect and extract from the EUV data. The motivation for this mainly originates from the fact that SDO has no coronagraph

as part of its suite of instruments. Therefore, to be able to detect the launch of a CME, we are restricted to the analysis of low-coronal data, such as that which will be returned by AIA.

The presented algorithm is designed to extract coronal dimmings in the seven EUV passbands observed with the AIA instrument. Whilst most CMEs are associated with some detectable coronal dimming signature, it should be noted that if a CME is initiated very gradually from high in the corona it may not generate an EUV dimming detectable in passbands that view the lower corona. In such cases, it is unlikely that a dimming signature related to the CME can be detected in AIA data. Indeed, recently Robbrecht, Patsourakos, and Vourlidas (2009) reported the case of a *Solar and Terrestrial Relations Observatory* (STEREO)-observed CME without any obvious low-coronal signatures such as coronal dimming.

We endeavor to obtain as much information as possible concerning each dimming identified using our algorithm. We hope that this will assist the user in their analysis and interpretation of coronal-dimming signatures.

2. Existing Algorithms

The work reviewed in the following sub-sections constitutes the automatic/semi-automatic dimming detection and extraction algorithms of which the authors are currently aware.

2.1. NEMO Algorithm, Podladchikova *et al.* Work

The Novel EIT wave Machine Observing (NEMO) algorithm (Podladchikova and Berghmans, 2005), was developed as an on-disk eruption measuring tool for detecting solar eruptions automatically in *Solar and Heliospheric Observatory/Extreme ultra-violet Imaging Telescope* (SOHO/EIT) data. The NEMO software is based on analysis of the general statistical properties and underlying physics of eruptive on-disk events. It successfully detects the occurrence of coronal waves and dimmings by looking for a significant perturbation to the statistical distribution of the pixels of running-difference images. Higher-order moments of the distribution of the running-difference image pixels are calculated to detect coherent large-scale structure amid the noise. In particular, the variance and kurtosis (peakedness of the distribution) are used as indicators that an event of interest has occurred.

Coronal waves and expanding coronal dimmings associated with CMEs both alter a significant number of pixels. An assumption made by NEMO is that the dimmings are essentially larger than other areas of the Sun with low intensities. The NEMO detection method is most likely to fail for dimmings without EIT waves and highly corrupted images. This is because detecting a significant variation in the statistics of the images relies on the disruption of a large enough number of pixels. With a localized dimming only a small number of pixels are affected, and these may fail to produce a significant change in the full-Sun distribution.

After an event has been detected, the extraction of the dimmed pixels uses a method called "progressive growth" of the intensive dimming region. The extraction is carried out using base – difference data (where, after compensating for the solar rotation, a pre-event image is subtracted from all subsequent images). Two groups of pixels are collected: *i*) a maximal pixel map which contains all pixels below a relatively high intensity threshold (this map also contains noise), and *ii*) a minimal pixel map which contains just the darkest 1% of the pixels of the base-difference image. Noise is removed using a median filter (5×5), and the final dimming is formed by starting with the darkest 1% of the pixels and growing the region within the confines of the filtered maximal pixel map, maintaining the condition of a

simply-connected region. The right panel of Figure 4 is from Podladchikova and Berghmans (2005) and shows the main dimming region for the 12 May 1997 event, extracted using this region-growing method.

2.2. Bewsher *et al.* Work

The statistical study carried out by Bewsher, Harrison, and Brown (2008), and the algorithm developed for that work, concentrates on dimmings observed in SOHO/CDS data (Harrison *et al.*, 1995) that occur near the solar limb. Both the Fe XVI and Mg IX spectral lines are examined for coronal dimmings, representing temperatures of 1×10^6 and 2×10^6 K, respectively. Base – difference images are produced for each sequence of images studied. If the base – differenced intensity value of a given pixel is greater than twice the error then the pixel is noted as dimmed and neighboring pixels in space and time are examined, until the extent of a given dimming is established. A minimum group size of one hundredth the dimming mosaic area is used to limit the spatial extent of the dimmings of interest.

2.3. Aschwanden *et al.* (2009) Work

Aschwanden *et al.* (2009) describe their algorithm that measures the EUV peak intensity and coronal background intensity, and determines the geometric width of the dimming region. Their study (and algorithm) applies to dimmings that occur adjacent to an active region where the average local density or EUV intensity is enhanced above the surrounding coronal background. The intensity of the dimming region at times after the onset of dimming is also measured. From this information their algorithm calculates the volume of the coronal plasma where EUV dimming is detected, and the total mass of the plasma that has been removed after a CME launch.

This algorithm selects dimming events from CMEs observed in STEREO/COR2 data. Our algorithm presented in this paper for application to SDO/AIA data differs significantly in its purpose (although some of the outputs derived are similar), since our algorithm is designed to detect coronal dimming events without any prior information regarding a CME event such as a likely time interval or spatial location.

Aschwanden *et al.* (2009) parameterize the coronal-dimming volume by assuming a cylindrical geometry with a vertical extent (approximated by one density scale height) and a circular footpoint area, based on the observed angular extent of the dimming region. This method means that this algorithm does not retain information regarding the "ragged dimming profile". Whist this approximation may provide a robust estimate for the width of coronal dimmings that form near to an active region, Attrill *et al.* (2006), Crooker and Webb (2006), and Attrill *et al.* (2008) demonstrated that the evolution of the outermost edges of coronal dimming regions potentially contain valuable information regarding the development of the CME post-eruption, as well as data on how coronal dimmings recover.

3. Our Algorithm

3.1. Part 1: Detecting the Occurrence of a Coronal-Dimming Event

The detection part of our algorithm is based largely on the work of Podladchikova and Berghmans (2005) and the principle of operation behind the NEMO software discussed in Section 2.1, namely the analysis of statistical properties of the distribution of the pixels.

It is acknowledged independently by both the authors of this paper and E. Podladchikova (private communication, 2009), that any expanding dimming observed in the low corona, is also associated with a coronal wave. For example, even the smallest source region of a magnetic cloud ever observed (Mandrini *et al.*, 2005) had a coronal wave that occurred with the development of the associated coronal dimmings (see Figure 7).

Our implementation of the NEMO analysis technique differs in that we calculate the statistical properties of the original (non-differenced) images. As described in Section 2.1, NEMO calculates the statistics of running-difference images. The procedure for producing running-difference images requires compensating for the solar rotation before subtracting the previous image from the current one. Both of these steps require computing time. With our ultimate aim of running near real-time detection on AIA data, we investigated the possibility of running the detection algorithm on straightforward original intensity images. As we show below, using this technique it is indeed possible to detect the occurrence of a coronal-dimming event.

One of the difficulties noted by Podladchikova and Berghmans (2005) in analyzing the higher-order moments of the data associated with a dimming event, is that small events that only disrupt a limited number of pixels get lost in the distribution of the full-Sun images. In principle, it is possible to circumnavigate this issue by sub-dividing the solar images into smaller areas (*e.g.,* into quadrants or 16ths). In this way, disruption of a smaller number of pixels has a relatively larger impact on the distribution from a given region.

To test this principle, the smallest magnetic-cloud source region ever detected (studied by Mandrini *et al.*, 2005) was used as a test case. The dimming event identified as the source region of the magnetic cloud occurred on 11 May 1998. Calculating the higher-order moments based on the distribution of pixels from the full-Sun images, the event was not flagged. However, dividing the solar images into 16 sectors, the higher-order moments of the statistics for each sector were calculated, and two eruptions from this tiny source region were successfully detected at ≈06:34 UT and ≈08:12 UT. The kurtosis from the sector where the source region was located is shown in Figure 2. Figure 7 shows difference images of the event as well as the subsequent extraction of the dimming region, following the successful detection.

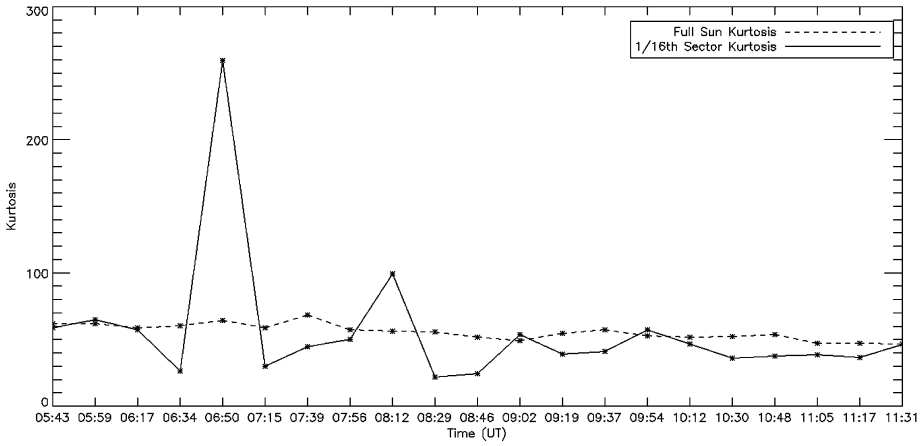

Figure 2 Kurtosis of the original EIT intensity data for the 11 May 1998 smallest magnetic cloud event source eruption. Kurtosis values are plotted for *i*) the full-disk image (dashed line) and *ii*) the 1/16th sector at the location of the dimming source region (solid line).

By increasing the probability of the detection of small events, in principle we also increase the probability of detecting a spurious event. In addition to the observational test for the 11 May 1998 event described here, a detailed study of more small events is required to determine the ratio of "spurious/successful detections", and resolve this potential source of error. A characteristic of coronal dimmings associated with eruptive events is that they persist over an extended period of time (*e.g.,* Rust, 1983; Kahler and Hudson, 2001; Attrill *et al.*, 2008). For example, the 11 May 1998 dimmings showed a depleted mean intensity for at least two hours following the eruption at 08:12 UT (see Figure 7). It is this characteristic that most directly affords discrimination between a spurious event due to noise and a real dimming associated with an eruptive event.

The detection part of our algorithm was also tested on slow events, such as a slow-rise near-limb event studied by Goff *et al.* (2005). The CME still caused significant disruption to surrounding loop structures, so the event could be identified by a disturbance in the statistical distribution of the image pixels.

It is expected that the dimming-event detection part of the algorithm will run on full-disk data from the AIA 193 Å passband. This choice is influenced by the communities' experience in analyzing coronal dimmings using the 195 Å data provided by SOHO/EIT. During the commissioning phase, if it is found that coronal dimmings are better observed in the new AIA EUV passbands, then we will additionally use them to flag the occurrence of a coronal dimming event. Indeed, it may be the case that a complimentary pair of passbands returns a superior coverage of coronal dimming events. For example, Bewsher, Harrison, and Brown (2008) conclude that simultaneous monitoring across a broad range of lines in the range from 1 to several million K would perhaps be the best approach. To start with however, we will use data from the AIA 193 Å passband since its temperature response function peak spans this temperature range. Although the full-resolution AIA data will comprise 4096×4096 pixels, testing shows that the dimming detection works successfully on binned EIT and *Extreme Ultra-Violet Imager* (EUVI) 512×512 full-disk data. A cadence of ten minutes is sufficient for detecting the onset of an eruptive CME-associated dimming, as EIT 195 Å data testify.

3.2. Defining and Quantifying Coronal Dimming

The first step in considering how to extract coronal dimmings automatically after the occurrence of an event has been flagged, is to develop a working understanding of how a coronal dimming may be defined/quantified. Reinard and Biesecker (2008) present a semi-automatic method for describing coronal dimming. They define dim pixels as those that are more than 1σ below the mean value of an entire pre-event differenced image. We adopt this threshold and use base – difference images to identify regions of dimming.

As discussed in Section 1, a coronal dimming can be caused by:

i) A real "opening" of the corona, plasma is evacuated. Intensity level depleted.
ii) Removal of a bright feature (*e.g.,* sigmoid elbow, overlying loop, disappearance of scattered light). The first two elements can potentially contribute to the mass of a CME.
iii) A heating or cooling of the coronal plasma out of the passband used for observations.

In certain cases, it is possible to pick out *i*) in raw intensity data and identify a dimming (*e.g.,* see Figure 1). However, it is much more difficult to identify dimmings caused by *ii*) in this manner. Our experience (and indeed that recorded in the literature, *e.g.,* Delannée and Aulanier, 1999; Podladchikova and Berghmans, 2005; Chertok and Grechnev, 2005) strongly suggests that base – difference data are required for confident identification

of a coronal dimming. We emphasize that running-difference data do not provide a true representation of real brightenings and dimmings.

This detection technique, employing a threshold of 1σ below the mean value of the entire pre-event differenced image, is actually very sensitive – it picks out even non-eruptive dimmings.

After using base – difference images to extract a dimming region, our algorithm then returns to the original intensity data in order to properly quantify the identified change. From the original data, outputs such as light curves showing the intensity evolution within the region that undergoes dimming can be used to establish which regions dim significantly and abruptly. It is these that are most likely indicative of eruption source regions. Information on the evolution of the dimmings also shows whether the dimming is long lived, or if it recovers in intensity fairly rapidly. This information also allows the algorithm to account for bad pixels, which tend to only appear in single frames, and as such have a minimal "lifetime" (see, *e.g.,* Figure 7).

3.3. Part 2: Extracting Coronal Dimming Regions

Having identified the onset of an eruptive dimming event using the dimming detection method described in Section 3.1, the dimming-extraction module will be triggered. The dimming extraction module will select an image before the dimming detection to act as a pre-event (base, reference) image. The images in the hours following this base image are then de-rotated to the time of the base image. Base – difference images (where the pre-event base reference image is subtracted from all subsequent images) are then created using binned 512×512 data from each of the seven EUV passbands onboard AIA. The mean value of the pre-event base – difference reference image in each passband is then calculated and the 1σ threshold suggested by Reinard and Biesecker (2008) (described in Section 3.2) is applied to identify the dimmed pixels.

Following identification of the dimmed pixels, median-filter smoothing is employed which replaces each point with the median of the two-dimensional neighborhood of a given number of pixels (we use a 3×3 filter). It is similar to smoothing with a boxcar or average filter but does not blur edges larger than the neighborhood. In addition the median filtering effectively removes noise in the form of isolated high or low values.

For each base – difference image in the de-rotated set, a mask of all dimmed pixels is created for each time frame. Dimming regions are then defined to be those pixels that are clustered in a neighborhood (using IDL's `label_region`). We discard regions that have an area less than 1 arc min^2. This is a somewhat arbitrary level, but this filter removes noise and still identifies the smallest source-region of a magnetic cloud known to date (Mandrini *et al.*, 2005, and see Figure 7).

If the user wishes to study dimming regions with a spatial extent smaller than this threshold of 1 arc min^2, then the pre-threshold dimmings identified by the algorithm remain available as an output. For example, the 11 April 2006 eruption, which was observed as a magnetic cloud at 1 AU (Steed *et al.*, 2008), had barely any source-region signatures such as coronal dimming discernable from a visual inspection of the data. However, on running our algorithm on this data set from EIT, coronal dimmings associated with the source region of this event are successfully identified. The area of the coronal dimming does not exceed the 1 arc min^2 threshold set in our algorithm, so the region is not automatically extracted from the identified dimmings. The application of our algorithm to this event illustrates the importance of automated identification of coronal dimmings. The results provide further support for the tiny region that Steed *et al.* (2008) identified as the source region of the magnetic cloud which arrived at 1 AU just 59 hours after the development of the coronal dimmings.

3.4. Metadata Outputs

Once the dimming regions have been identified, various metadata are extracted for each region, including:

- *Area*. The area of each dimming region is recorded, and the time at which the dimmings occupy a maximum area is automatically identified.
- *Light curves*. The mask that corresponds to the time of maximum dimming area is used to construct light curves (using original de-rotated intensity data). The light curves show the intensity evolution of the pixels of each region identified with the maximum dimming area mask. Figure 7 shows an example of this output.
- *Location of dimming* (the center of each dimming region is calculated). It is important to have information concerning the location of each dimming region because outputs such as lifetime will be artificially shortened the further the source region is located to the West, because they will disappear around the west limb faster. Additionally, due to their location near to the west limb, these regions will be subject to artificial brightening which is an artefact of de-rotation.
- *Volume* (from information on the depth of the dimming). It is important when calculating the volume to look at changes in the real intensity, not just the base – differenced data (this will be discussed further in Section 4). Quantities such as *i*) the relative dimming percentage, *ii*) the pre-event intensity of a region which subsequently is identified as a coronal dimming, and *iii*) the evolution of the intensity of a dimming with time, are important to enable confident identification of real dimming, rather than just a fluctuation in intensity (*e.g.,* of an active region). This information also allows identification of bad pixels (because the "dimmings" in this case would be short-lived on timescales of just one frame, see, *e.g.,* Figure 7).
  The volumes of the dimmings can be calculated by considering the intensity change in the original data for the dimmed regions. In contrast to observations of coronal dimmings with *Yohkoh*/SXT data (Kahler and Hudson, 2001), we note that in EUV data coronal dimmings are observed to have a non-uniform intensity (Attrill *et al.*, 2008). Rather, the dimmings are highly structured and exhibit a complex recovery – they recover from shrinking from the external boundary as well as brightening internally. Therefore, if one wishes to study the recovery phase of coronal dimmings, it is important that the extracted region is not over-smoothed, but that information is retained concerning the fragmentary outer boundary of the actual dimming region, as well as internal structure. Our algorithm preserves this information (see, *e.g.,* Figures 5 and 9).
- *Mass*. Ultimately, the total mass from the coronal dimming regions will need to be synthesized from multiple temperature filters (Aschwanden *et al.*, 2009). When calculating the density of the plasma in each of the different passbands observed by AIA, we will need to ascertain the corresponding altitude and density scale height of the source of the plasmas seen in the different passbands. This is because the bulk of the coronal plasma is distributed over a thermal scale height, and a reasonable estimate of the altitude of the centroid of the dimming plasma is a half density scale height, which is temperature dependent (Aschwanden *et al.*, 2009).

4. Test Cases

We present examples of both simple and complex dimming events extracted using our algorithm. Contrasting events at both the minimum and maximum of solar cycle 23 are iden-

tified in SOHO/EIT data. A more recent event extracted from STEREO/EUVI data is also presented, demonstrating the potential for the anticipated application to SDO/AIA data.

4.1. Extracting Dimmings from SOHO/EIT Data

4.1.1. Solar Minimum Simple Event – 12 May 1997

Dimming onset is identified at 04:50 UT by the detection method described in Section 3.1. The dimmings are extracted using the main algorithm (Sections 3.2 and 3.3). Both the base – difference data and resulting dimming masks are shown in Figure 3. The 12 May 1997 event was selected as a simple test case because there is considerable existing work regarding the dimmings of this event, both observational and based on existing automatic detection methods. A comparison of the region extracted by our algorithm with the regions defined by existing options is shown in Figure 4. Comparison with the observationally-defined contour method described in Attrill *et al.* (2006) and the NEMO extraction from Podladchikova and Berghmans (2005) are shown. The similar results between our algorithm and these existing methods is encouraging.

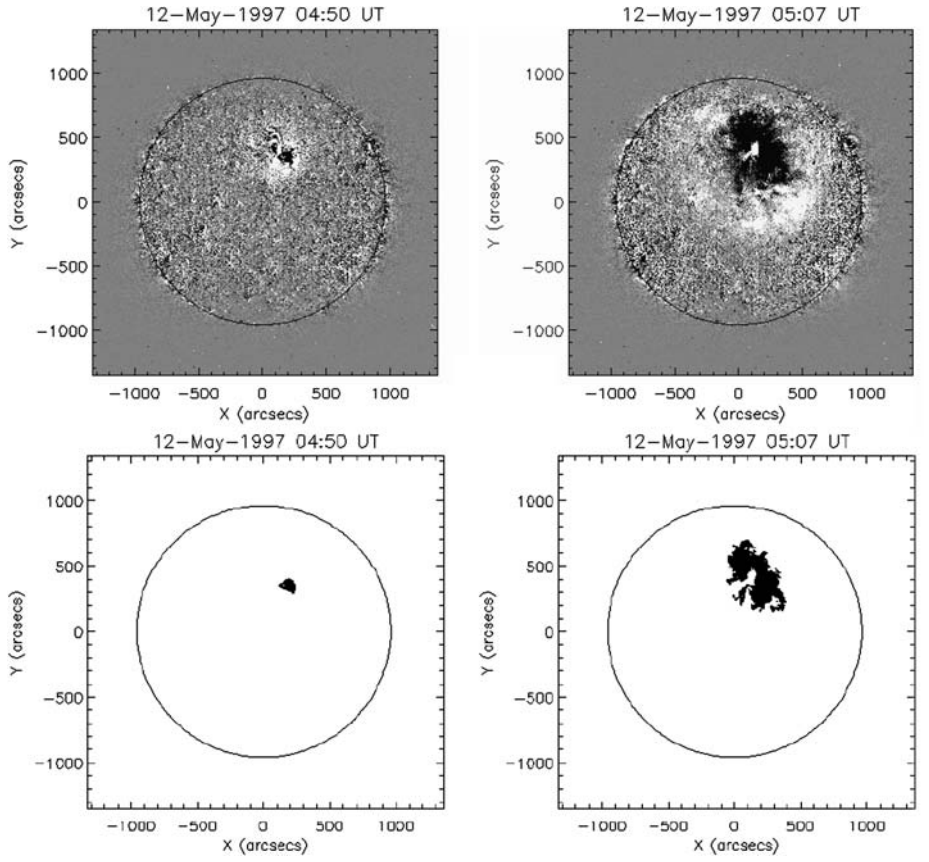

Figure 3 The top and third rows show base – difference images of the early phases of the 12 May 1997 dimming and coronal-wave event. The second and bottom rows show the corresponding dimmed pixels extracted by our algorithm.

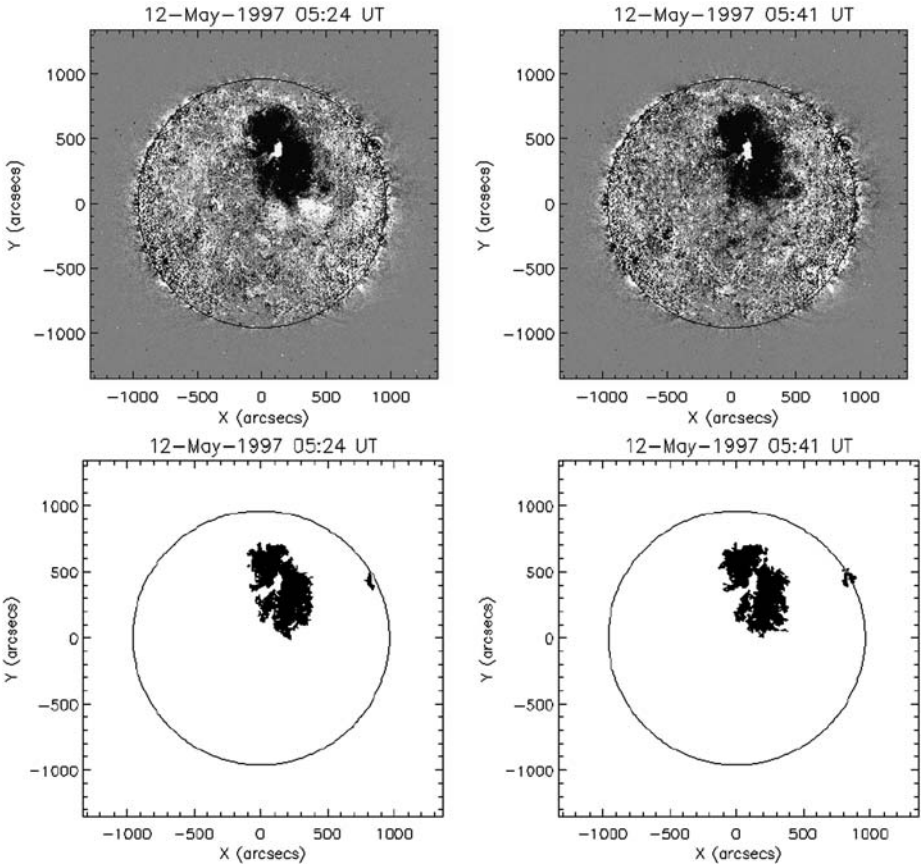

Figure 3 (*Continued.*)

Making the assumption that the quiet coronal height of 100 Mm (one pressure scale height) is analogous to the intensity of the majority of the pixels in the pre-event data, the corresponding column depth for each pixel is normalized with respect to this value.

The mass contained in a volume V is $m = m_p n V$, where m_p is the proton mass (the corona is assumed to be fully ionized hydrogen plasma), and n is the number density. Considering densities in the range 5×10^8 cm^{-3} – 1×10^9 cm^{-3}, for the dimmings at their maximum spatial extent (05:41 UT on 12 May 1997), our algorithm returns a mass ranging from 6×10^{15} – 1×10^{16} g. The result returned by the mass calculation depends heavily on the density selected (*e.g.,* Aschwanden *et al.*, 2009) find a coronal background density of 2.7 ± 0.3 $\times10^8$ cm^{-3} for the STEREO/EUVI 195 Å wavelength. Using this density, the mass estimate would be revised to 3×10^{15} g).

For comparison, Zhukov and Auchère (2004) performed a DEM analysis of a similar region for this event and found that 1.4×10^{15} g erupts from the whole dimming region. Considering that both of these calculations provide only rough order-of-magnitude estimates, as well as the substantially different approaches adopted, there is a fair agreement between these values. We were unable to find estimates for the mass of the associated CME for this event, though Howard *et al.* (1985) studied 998 white-light CMEs and report masses ranging between 2×10^{14} g – 4×10^{16} g.

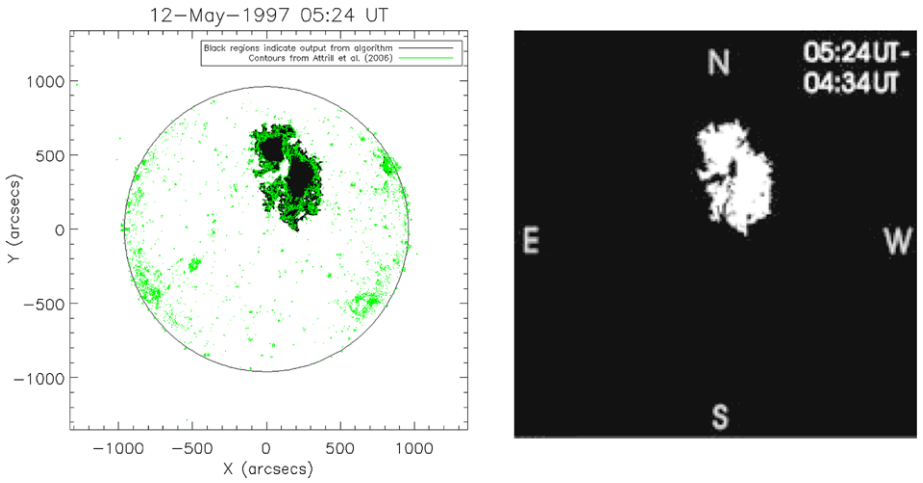

Figure 4 Left panel shows the extracted output from our algorithm at 05:24 UT, overlaid with green contours using the method described in the observational study by Attrill *et al.* (2006). Right panel shows the dimming region extracted using the automatic region-growing method described by Podladchikova and Berghmans (2005).

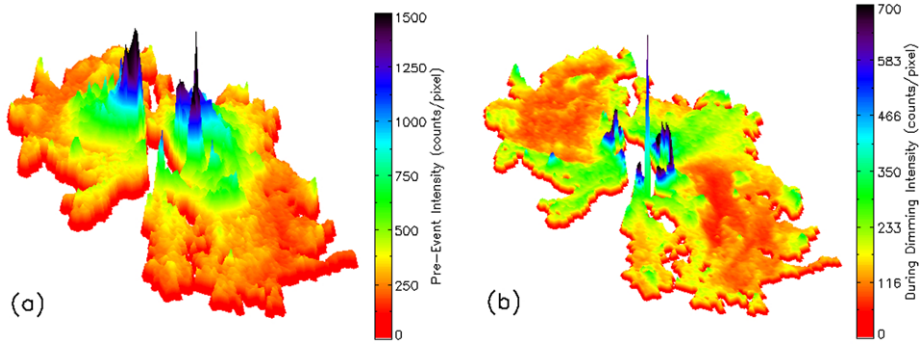

Figure 5 3D surface plots showing the main dimming region extracted by the algorithm for the 12 May 1997 event. Left panel shows the pre-event intensity of the pixels that later dim. Right panel shows the intensity of the pixels during the dimming at 05:41 UT.

4.1.2. Solar Maximum Complex Event – 28 October 2008

The dimming onset in this event is identified at 10:14 UT. The main flare with this event occurs at ≈11:11 UT (Mandrini *et al.*, 2007), although significant activity was already underway prior to this X17 flare (*e.g.,* see Mandrini *et al.*, 2006). Consistent with this, on completion of running the main extraction algorithm, it becomes clear that dimmings also occurred just prior to the main flare event and global dimmings.

Figure 6 shows base-difference data and the extracted dimming regions that are associated with activity both at 10:14 UT, prior to the X17 flare, as well as the global dimmings that developed during the main eruption.

A difference between the NEMO algorithm and our extraction method is that our algorithm can be run on EUV data that contain information about the corona above the limb.

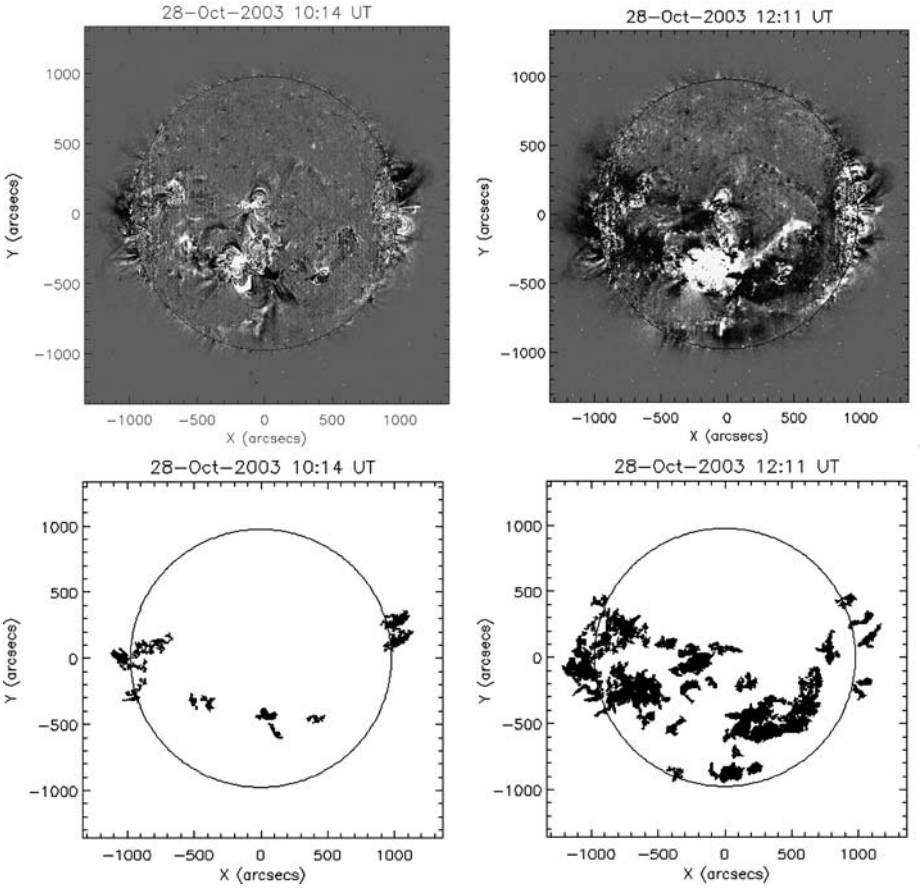

Figure 6 The complex 28 October 2003 coronal dimmings. This event was part of a series of exceptionally powerful eruptions known as the "Halloween events". Top panels show base – difference images at 10:14 UT pre-flare (left panel) and 12:11 UT, at the maximum area of the dimmings. Bottom panels show the dimmings extracted by our algorithm.

To our knowledge, NEMO concentrates on extracting on-disk dimming regions only. Recent work with this particular 28 October 2003 event (Mandrini *et al.*, 2007), highlights the importance of off-limb dimmings in developing an understanding of this event. Mandrini *et al.* (2007) measure the magnetic flux through the on-disk dimmings present on 28 October 2003. They find a significant imbalance in the net magnetic flux, which they conclude can only be resolved by considering the contribution from a large coronal dimming that develops over the east limb during the event.

Using a density range of $5\times10^{8}-1\times10^{9}$ cm^{-3}, our algorithm determines an erupted mass of $1.4-2.3\times10^{16}$ g from the extracted dimming regions shown in Figure 6 at 12:11 UT. Jackson *et al.* (2007) report a total mass of 8.3×10^{16} g for this CME, from analysis of *Solar Mass Ejection Imager* (SMEI) data. The authors of that work note that the SMEI reconstructed data returns a mass a factor of two to three larger than that determined from LASCO/C3 observations.

Our algorithm identifies dimming regions that have myriad shapes. It is particularly evident when analyzing this event that the assumption of a circular geometry for the coronal dimmings would deviate significantly from the observations. Another feature of this event is that coronal dimmings associated with the eruption develop right across the solar disk (and off-limb), at locations remote from the active region where the associated flare is observed to occur (white region at $\approx[-100, -400]$ in the top right panel of Figure 6). We note that the inclusion of these extended secondary dimming regions in the extraction differs from the approach described by Aschwanden *et al.* (2009) who use the full width of the active region as a measure of the width of the EUV dimming region.

4.1.3. Very Small Event – 11 May 1998

In searching for extreme events, as well as more typical ones with which to test our algorithm, we chose the 11 May 1998 eruption studied by Mandrini *et al.* (2005) which is known as the smallest magnetic cloud source region identified (with the exception of the recent study by Steed *et al.* (2008) already discussed in Section 3.3). The 11 May 1998 event is an excellent test case for our algorithm to see if it successfully identifies the smallest coronal dimmings associated with a known magnetic-cloud event.

Figure 7 shows the output of our algorithm at 08:46 UT. The source region coronal dimmings are successfully identified (highlighted by the red box in the middle panel of Figure 7). Also shown in this image are corrupted pixels (indicated by the "dimming" surrounded by a blue dashed box in the middle right panel of Figure 7). The bottom panel of Figure 7 shows the light curves from both these dimming regions. The corrupted pixels show up only in one frame, and hence are easily identified as not being a real coronal dimming. On the other hand, the source-region coronal dimming (red curve) is substantial and exhibits a gradual recovery consistent with existing analysis of other coronal dimmings (*e.g.,* Attrill *et al.*, 2008). The mass returned by our algorithm for this tiny event is $2.4-4.8\times10^{15}$ g. Since CMEs typically have masses of $\approx10^{15}$ g, this estimate of the mass removed from the coronal dimming regions is consistent with an event toward the lower end of the spectrum.

4.2. Extracting Dimmings from STEREO/EUVI Data – 26 April 2008

To illustrate the algorithm when applied to STEREO/EUVI data, we select an event on 26 April 2008, a global-scale coronal-wave – CME – dimming event. We analyze the data from STEREO Behind. Figure 8 shows the 195 Å base-difference image at 14:26 UT, along with the output from our algorithm showing the extracted dimming regions. The extracted dimming area seems to be larger than the main dimmings visible near to the post-eruptive arcade in the base-difference image. Our algorithm extracts all pixels that show a decrease in intensity of more than 1σ below the mean intensity level of the pre-event base-difference image. As noted earlier, this threshold is very sensitive and identifies even relatively shallow dimmings. It is for this reason that it is important to calculate the magnitude of the intensity change (and subsequently the volume and mass) using non-differenced EUVI data. Also visible in the base – difference data is a remnant part of the coronal-wave bright front that occurred in association with this dimming event. The patchy, white brightenings can be seen near to the central meridian in the left panel of Figure 8.

Figures 9(a) and (b) show 3D surface plots of the non-differenced pre-event and during-dimming (at 14:26 UT) EUVI data, for the pixels extracted by the algorithm. Figure 9(b) reveals that the deepest dimming does not occupy all of the extracted pixels. Rather the deepest dimmings (red regions) are located to the East of the post-eruptive arcade, with a

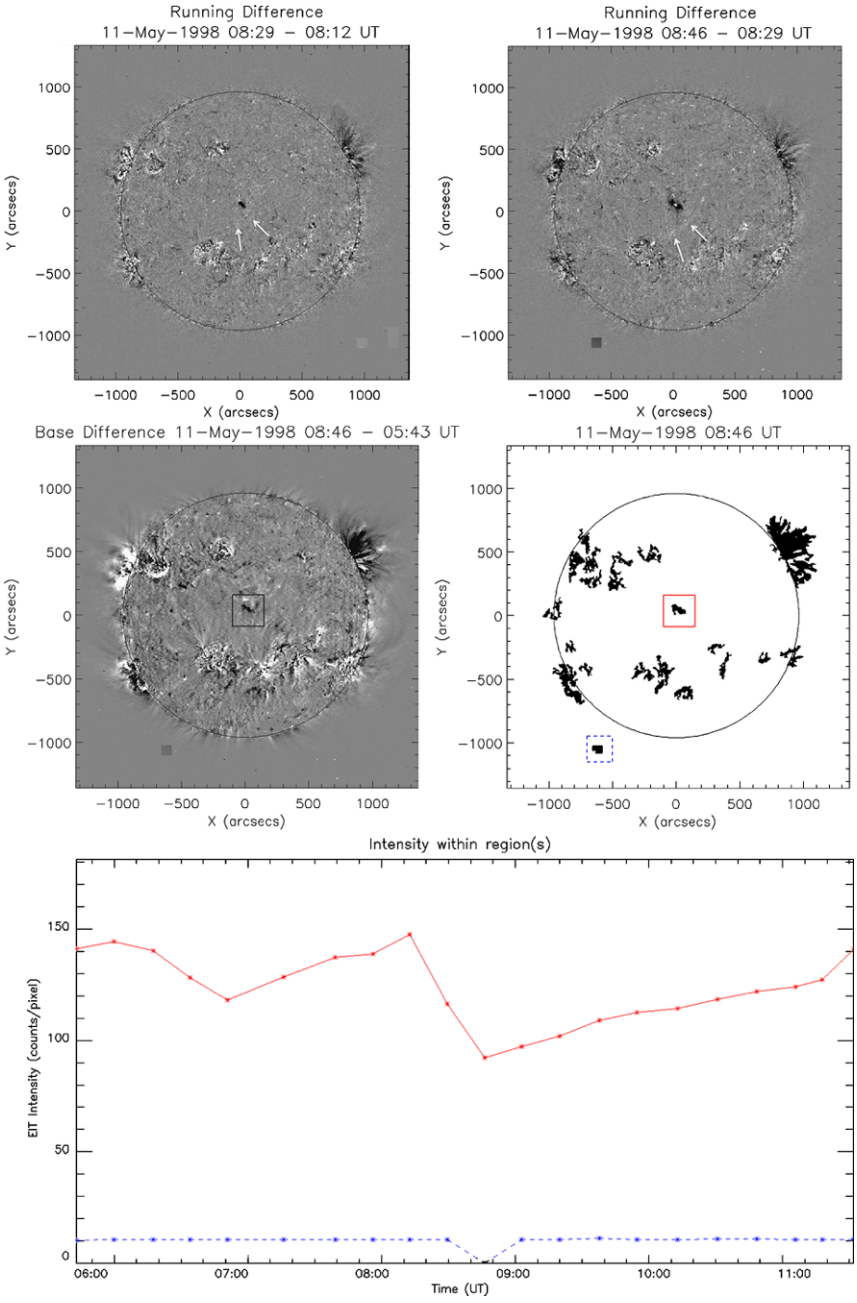

Figure 7 Top panels shows running-difference images of the 11 May 1998 eruption. White arrows indicate the coronal wave associated with this event. Middle left panel is a base – difference image showing the coronal dimmings identified (in the black box) as the smallest source region of a magnetic cloud ever observed by Mandrini *et al.* (2005). Middle right panel shows the coronal dimmings extracted by our algorithm. The dimmings in the red box (solid line) correspond to the source region of the event. The "dimming" in the blue dashed box are corrupted pixels. The bottom panel shows the light curves derived from the average intensity of the pixels in the source dimming (red, solid) and corrupt pixels (blue, dashed).

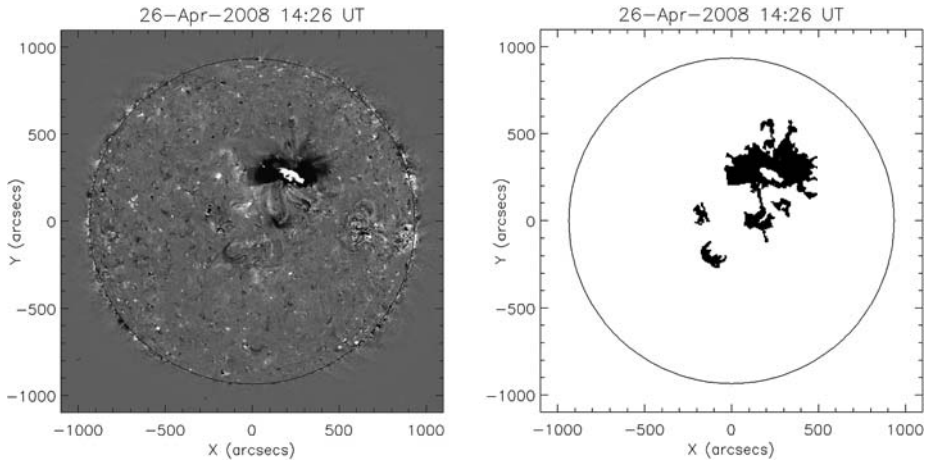

Figure 8 Left panel shows a STEREO/EUVI 195 Å base – difference image from spacecraft B at 14:26 UT on 26 April 2008. A remnant part of the bright coronal-wave front (white patches near central meridian) are visible, as well as the coronal dimmings (black regions). Right panel shows the dimmed pixels extracted by our algorithm.

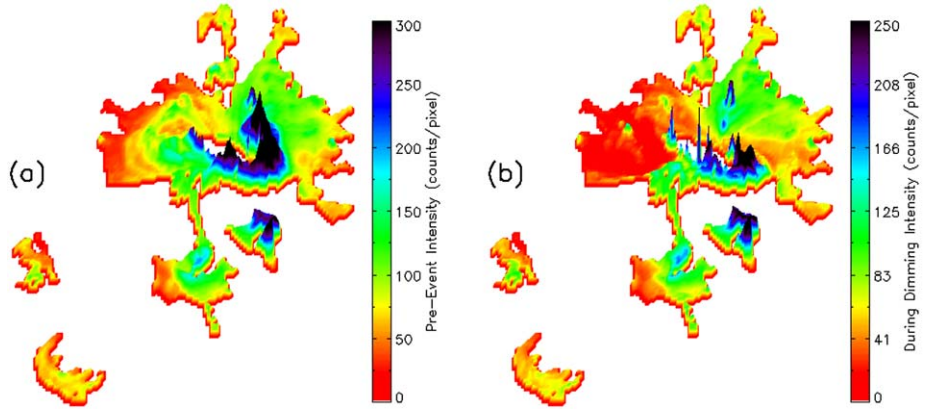

Figure 9 3D surface plots showing the dimming regions extracted by our algorithm for the 26 April 2008 event, observed by STEREO/EUVI B. Left panel shows the pre-event intensity of the pixels that later dim. Right panel shows the intensity of the pixels during the early stages of the dimming event at 14:26 UT.

smaller region to the West. The rest of the extracted region consists of a less pronounced dimming, indicated by the yellow and green regions.

The mass calculated from the dimmings extracted at 14:26 UT is $2.7-6.0\times10^{15}$ g. The eruption on 26 April 2008 was a global-scale event, and the mass calculated when the dimmings reached their maximum spatial extent at 15:56 UT, (after the coronal-wave had expanded across the disk) is $4.0\times10^{15}-1.0\times10^{16}$ g.

5. Summary

The coronal dimming detection and extraction algorithm described in this paper is part of the SDO/*Computer Vision Center* effort hosted at SAO (Martens *et al.*, 2009), to assist with organizing the vast amount of data anticipated from SDO/AIA.

Our algorithm has been designed by building on existing pioneering works concerning the automatic detection of coronal dimmings in EUV imager data. The resulting product differs significantly from existing tools, specifically our algorithm is capable of analyzing: both disk and limb dimmings, myriad shapes and sizes of dimming, as well as secondary dimmings that develop remote from an initial source region. The next required step is to examine more events in order to determine the ratio of "spurious/successful detections". This is particularly important for confident identification of small dimming events.

We have demonstrated that the detection part of the code can run on non-differenced data, ensuring that it can run in near real-time, as soon as the calibrated data products are available. The whole spectrum of known events, from solar minimum to maximum, can be successfully detected.

We have also demonstrated the proof-of-concept for the anticipated application to AIA data, using examples from both EIT and EUVI datasets. The main extraction algorithm is anticipated to be run on all seven EUV passbands of AIA data, in order to refine estimates of the mass of coronal dimmings.

We hope that this algorithm and metadata output will greatly assist efforts to assemble large-scale statistical studies of coronal dimming regions.

Acknowledgements We sincerely thank the anonymous referee for suggestions that improved the description of the work presented here, as well as for helpful comments pertinent to the next phase of testing and development. We are grateful to E. Podladchikova, D. Bewsher, S. Saar, P. Grigis, and A. Davey for helpful discussions. We acknowledge NASA grant NNX08BA97G, which supported this work.

References

Aschwanden, M.J., Wuelser, J.P., Nitta, N.V., Lemen, J.R., Sandman, A.: 2009, First three-dimensional reconstructions of coronal loops with the STEREO A + B spacecraft. III. Instant stereoscopic tomography of active regions. *Astrophys. J.* **695**, 12 – 29. doi:10.1088/0004-637X/695/1/12.

Attrill, G., Nakwacki, M.S., Harra, L.K., van Driel-Gesztelyi, L., Mandrini, C.H., Dasso, S., Wang, J.: 2006, Using the evolution of coronal dimming regions to probe the global magnetic field topology. *Solar Phys.* **238**, 117 – 139. doi:10.1007/s11207-006-0167-5.

Attrill, G.D.R., Harra, L.K., van Driel-Gesztelyi, L., Démoulin, P., Wülser, J.P.: 2007, Coronal "wave": A signature of the mechanism making CMEs large-scale in the low corona? *Astron. Nachr.* **328**, 760 – 763. doi:10.1002/asna.200710794.

Attrill, G.D.R., van Driel-Gesztelyi, L., Démoulin, P., Zhukov, A.N., Steed, K., Harra, L.K., Mandrini, C.H., Linker, J.: 2008, The recovery of CME-related dimmings and the ICME's enduring magnetic connection to the Sun. *Solar Phys.* **252**, 349 – 372. doi:10.1007/s11207-008-9255-z.

Bewsher, D., Harrison, R.A., Brown, D.S.: 2008, The relationship between EUV dimming and coronal mass ejections. I. Statistical study and probability model. *Astron. Astrophys.* **478**, 897 – 906. doi:10.1051/0004-6361:20078615.

Chertok, I.M., Grechnev, V.V.: 2003, Large-scale dimmings produced by solar coronal mass ejections according to SOHO/EIT data in four EUV lines. *Astron. Rep.* **47**, 934 – 945. doi:10.1134/1.1626196.

Chertok, I.M., Grechnev, V.V.: 2005, Large-scale activity in the Bastille Day 2000 solar event. *Solar Phys.* **229**, 95 – 114. doi:10.1007/s11207-005-3654-1.

Crooker, N.U., Webb, D.F.: 2006, Remote sensing of the solar site of interchange reconnection associated with the May 1997 magnetic cloud. *J. Geophys. Res.* **111**, 8108 – 8114. doi:10.1029/2006JA011649.

Delannée, C., Aulanier, G.: 1999, CME associated with transequatorial loops and a bald patch flare. *Solar Phys.* **190**, 107 – 129.

Démoulin, P.: 2008, A review of the quantitative links between CMEs and magnetic clouds. *Ann. Geophys.* **26**, 3113 – 3125.

Goff, C.P., van Driel-Gesztelyi, L., Harra, L.K., Matthews, S.A., Mandrini, C.H.: 2005, A slow coronal mass ejection with rising X-ray source. *Astron. Astrophys.* **434**, 761 – 771. doi:10.1051/0004-6361:20042321.

Harrison, R.A., Lyons, M.: 2000, A spectroscopic study of coronal dimming associated with a coronal mass ejection. *Astron. Astrophys.* **358**, 1097 – 1108.

Harrison, R.A., Sawyer, E.C., Carter, M.K., Cruise, A.M., Cutler, R.M., Fludra, A., Hayes, R.W., Kent, B.J., Lang, J., Parker, D.J., Payne, J., Pike, C.D., Peskett, S.C., Richards, A.G., Gulhane, J.L., Norman, K., Breeveld, A.A., Breeveld, E.R., Al Janabi, K.F., McCalden, A.J., Parkinson, J.H., Self, D.G., Thomas, P.D., Poland, A.I., Thomas, R.J., Thompson, W.T., Kjeldseth-Moe, O., Brekke, P., Karud, J., Maltby, P., Aschenbach, B., Bräuninger, H., Kühne, M., Hollandt, J., Siegmund, O.H.W., Huber, M.C.E., Gabriel, A.H., Mason, H.E., Bromage, B.J.I.: 1995, The coronal diagnostic spectrometer for the solar and heliospheric observatory. *Solar Phys.* **162**, 233 – 290. doi:10.1007/BF00733431.

Howard, R.A., Sheeley, N.R. Jr., Michels, D.J., Koomen, M.J.: 1985, Coronal mass ejections – 1979 – 1981. *J. Geophys. Res.* **90**, 8173 – 8191.

Hudson, H.S., Cliver, E.W.: 2001, Observing coronal mass ejections without coronagraphs. *J. Geophys. Res.* **106**, 25199 – 25214. doi:10.1029/2000JA004026.

Hudson, H.S., Webb, D.F.: 1997, *Soft X-Ray Signatures of Coronal Ejections*, *Geophys. Monogr. Ser.*, AGU, Washington.

Hudson, H.S., Acton, L.W., Freeland, S.L.: 1996, A long-duration solar flare with mass ejection and global consequences. *Astrophys. J.* **470**, 629 – 635. doi:10.1086/177894.

Jackson, B.V., Hick, P.P., Buffington, A., Bisi, M.M., Kojima, M., Tokumaru, M.: 2007, Comparison of the extent and mass of CME events in the interplanetary medium using IPS and SMEI Thomson scattering observations. *Astron. Astrophys. Trans.* **26**, 477 – 487. doi:10.1080/10556790701612221.

Kahler, S.W., Hudson, H.S.: 2001, Origin and development of transient coronal holes. *J. Geophys. Res.* **106**, 29239 – 29248. doi:10.1029/2001JA000127.

Mandrini, C.H., Pohjolainen, S., Dasso, S., Green, L.M., Démoulin, P., van Driel-Gesztelyi, L., Copperwheat, C., Foley, C.: 2005, Interplanetary flux rope ejected from an X-ray bright point. The smallest magnetic cloud source-region ever observed. *Astron. Astrophys.* **434**, 725 – 740. doi:10.1051/0004-6361:20041079.

Mandrini, C.H., Demoulin, P., Schmieder, B., Deluca, E.E., Pariat, E., Uddin, W.: 2006, Companion event and precursor of the X17 flare on 28 October 2003. *Solar Phys.* **238**, 293 – 312. doi:10.1007/s11207-006-0205-3.

Mandrini, C.H., Nakwacki, M.S., Attrill, G., van Driel-Gesztelyi, L., Démoulin, P., Dasso, S., Elliott, H.: 2007, Are CME-related dimmings always a simple signature of interplanetary magnetic cloud footpoints? *Solar Phys.* **244**, 25 – 43. doi:10.1007/s11207-007-9020-8.

Martens, P.C.H., Davey, A.R., Grigis, P.C., Kasper, J., Korreck, K., Saar, S.H., Su, Y., Savcheva, A., Testa, P., Wills-Davey, M., Bernasconi, P.N., Georgoulis, M.K., Delouille, V.A., Hochedez, J.F., Cirtain, J.W., DeForest, C.E., Angryk, R.A., De Moortel, I., Wiegelmann, T.: 2009, Computer vision for the solar dynamics observatory. *Solar Phys*., submitted.

Podladchikova, O., Berghmans, D.: 2005, Automated detection of EIT waves and dimmings. *Solar Phys.* **228**, 265 – 284. doi:10.1007/s11207-005-5373-z.

Qiu, J., Hu, Q., Howard, T.A., Yurchyshyn, V.B.: 2007, On the magnetic flux budget in low-corona magnetic reconnection and interplanetary coronal mass ejections. *Astrophys. J.* **659**, 758 – 772. doi:10.1086/512060.

Reinard, A.A., Biesecker, D.A.: 2008, Coronal mass ejection-associated coronal dimmings. *Astrophys. J.* **674**, 576 – 585. doi:10.1086/525269.

Robbrecht, E., Patsourakos, S., Vourlidas, A.: 2009, No trace left behind: STEREO observation of a coronal mass ejection without low coronal signatures. *Astrophys. J.* **701**, 283 – 291. doi:10.1088/0004-637X/701/1/283.

Rust, D.M.: 1983, Coronal disturbances and their terrestrial effects (Tutorial Lecture). *Space Sci. Rev.* **34**, 21 – 36.

Rust, D.M., Hildner, E.: 1976, Expansion of an X-ray coronal arch into the outer corona. *Solar Phys.* **48**, 381 – 387.

Steed, K., Owen, C.J., Harra, L.K., Green, L.M., Dasso, S., Walsh, A.P., Démoulin, P., van Driel-Gesztelyi, L.: 2008, Locating the solar source of 13 April 2006 magnetic cloud. *Ann. Geophys.* **26**, 3159 – 3168.

Sterling, A.C., Hudson, H.S.: 1997, YOHKOH SXT observations of X-ray "Dimming" associated with a halo coronal mass ejection. *Astrophys. J. Lett.* **491**, 55 – 58. doi:10.1086/311043.

Thompson, B.J., Plunkett, S.P., Gurman, J.B., Newmark, J.S., St. Cyr, O.C., Michels, D.J.: 1998, SOHO/EIT observations of an Earth-directed coronal mass ejection on May 12, 1997. *Geophys. Res. Lett.* **25**, 2465 – 2468. doi:10.1029/98GL50429.

Thompson, B.J., Cliver, E.W., Nitta, N., Delannée, C., Delaboudinière, J.P.: 2000, Coronal dimmings and energetic CMEs in April – May 1998. *Geophys. Res. Lett.* **27**, 1431 – 1434. doi:10.1029/1999GL003668.

Wang, T., Yan, Y., Wang, J., Kurokawa, H., Shibata, K.: 2002, The large-scale coronal field structure and source region features for a halo coronal mass ejection. *Astrophys. J.* **572**, 580 – 597. doi:10.1086/340189.

Webb, D.F., Lepping, R.P., Burlaga, L.F., DeForest, C.E., Larson, D.E., Martin, S.F., Plunkett, S.P., Rust, D.M.: 2000, The origin and development of the May 1997 magnetic cloud. *J. Geophys. Res.* **105**, 27251 – 27260. doi:10.1029/2000JA000021.

Wills-Davey, M.J.: 2006, Tracking large-scale propagating coronal wave fronts (EIT waves) using automated methods. *Astrophys. J.* **645**, 757 – 765. doi:10.1086/504144.

Zhukov, A.N., Auchère, F.: 2004, On the nature of EIT waves, EUV dimmings and their link to CMEs. *Astron. Astrophys.* **427**, 705 – 716. doi:10.1051/0004-6361:20040351.